Supplementary Material
Adversarial Attack Generation Empowered by Min-Max Optimization

Abstract

In this supplementary material, we first provide technical proofs of Proposition 1 and Lemma 1 in Sec A and B. We then discuss the proposed AMPGD algorithm in Sec C. In the next section, we show the details of experimental setup including the model architectures and training details in Sec D.1, the hyperparameters to craft the adversarial examples (Sec D.2), the details of data transformations (Sec D.3). Then we show additional experiments results for robust adversarial attacks (Sec E) and generalized adversarial training (Sec F). Finally, we provide more visualizations to show that domain weights $\mathbf{w}$ provide a holistic tool to interpret "image robustness" in Sec G. The summary of contents in the supplementary is provided in the following.

Contents

A Proof of Proposition 1

Proposition 1. *Given a point* $\mathbf{a} \in \mathbb{R}^d$ *and a constraint set* $\mathcal{X} = \{\boldsymbol{\delta} | \|\boldsymbol{\delta}\|_p \leq \epsilon, \check{\mathbf{c}} \leq \boldsymbol{\delta} \leq \hat{\mathbf{c}}\}$*, the Euclidean projection* $\boldsymbol{\delta}^* = \operatorname{proj}_{\mathcal{X}}(\mathbf{a})$ *has the closed-form solution when* $p \in \{0, 1, 2\}$*.*

1) If $p = 1$*, then* $\boldsymbol{\delta}^*$ *is given by*

$$\delta_i^* = \begin{cases} P_{[\check{c}_i, \hat{c}_i]}(a_i) & \sum_{i=1}^d |P_{[\check{c}_i, \hat{c}_i]}(a_i)| \leq \epsilon \\ P_{[\check{c}_i, \hat{c}_i]}(\operatorname{sign}(a_i) \max\{|a_i| - \lambda_1, 0\}) & \textit{otherwise}, \end{cases} \tag{14}$$

where $\mathbf{x}_i$ *denotes the* i*th element of a vector* $\mathbf{x}$*;* $P_{[\check{c}_i, \hat{c}_i]}(\cdot)$ *denotes the clip function over the interval* $[\check{c}_i, \hat{c}_i]$*;* $\operatorname{sign}(x) = 1$ *if* $x \geq 0$*, otherwise* 0*;* $\lambda_1 \in (0, \max_i |a_i| - \epsilon/d]$ *is the root of* $\sum_{i=1}^d |P_{[\check{c}_i, \hat{c}_i]}(\operatorname{sign}(a_i) \max\{|a_i| - \lambda_1, 0\})| = \epsilon$*.*

2) If $p = 2$*, then* $\boldsymbol{\delta}^*$ *is given by*

$$\delta_i^* = \begin{cases} P_{[\check{c}_i, \hat{c}_i]}(a_i) & \sum_{i=1}^d (P_{[\check{c}_i, \hat{c}_i]}(a_i))^2 \leq \epsilon^2 \\ P_{[\check{c}_i, \hat{c}_i]}\left(a_i/(\lambda_2 + 1)\right) & \textit{otherwise}, \end{cases} \tag{15}$$

where $\lambda_2 \in (0, \|\mathbf{a}\|_2/\epsilon - 1]$ *is the root of* $\sum_{i=1}^d (P_{[\check{c}_i, \hat{c}_i]}(a_i/(\lambda_2 + 1)))^2 = \epsilon^2$*.*

3) If $p = 0$ *and* $\epsilon \in \mathbb{N}_+$*, then* $\boldsymbol{\delta}^*$ *is given by*

$$\delta_i^* = \begin{cases} \delta_i' & \eta_i \geq [\boldsymbol{\eta}]_\epsilon \\ 0 & \textit{otherwise}, \end{cases} \qquad \eta_i = \begin{cases} \sqrt{2a_i\check{c}_i - \check{c}_i^2} & a_i < \check{c}_i \\ \sqrt{2a_i\hat{c}_i - \hat{c}_i^2} & a_i > \hat{c}_i \\ |a_i| & \textit{otherwise}. \end{cases} \tag{16}$$

where $[\boldsymbol{\eta}]_\epsilon$ *denotes the* ϵ*-th largest element of* $\boldsymbol{\eta}$*, and* $\delta_i' = P_{[\check{c}_i, \hat{c}_i]}(a_i)$*.*

Proof of Proposition 1:

ℓ_1 **norm** When we find the Euclidean projection of $\mathbf{a}$ onto the set $\mathcal{X}$, we solve

$$\begin{array}{ll} \underset{\boldsymbol{\delta}}{\text{minimize}} & \frac{1}{2}\|\boldsymbol{\delta} - \mathbf{a}\|_2^2 + I_{[\check{\mathbf{c}}, \hat{\mathbf{c}}]}(\boldsymbol{\delta}) \\ \text{subject to} & \|\boldsymbol{\delta}\|_1 \leq \epsilon, \end{array} \tag{17}$$

where $I_{[\check{\mathbf{c}}, \hat{\mathbf{c}}]}(\cdot)$ is the indicator function of the set $[\check{\mathbf{c}}, \hat{\mathbf{c}}]$. The Langragian of this problem is

$$L = \frac{1}{2}\|\boldsymbol{\delta} - \mathbf{a}\|_2^2 + I_{[\check{\mathbf{c}}, \hat{\mathbf{c}}]}(\boldsymbol{\delta}) + \lambda_1(\|\boldsymbol{\delta}\|_1 - \epsilon) \tag{18}$$

$$= \sum_{i=1}^d \left(\frac{1}{2}(\delta_i - a_i)^2 + \lambda_1|\delta_i| + I_{[\check{c}_i, \hat{c}_i]}(\delta_i)\right) - \lambda_1\epsilon. \tag{19}$$

The minimizer $\boldsymbol{\delta}^*$ minimizes the Lagrangian, it is obtained by elementwise soft-thresholding

$$\delta_i^* = P_{[\check{c}_i, \hat{c}_i]}(\operatorname{sign}(a_i) \max\{|a_i| - \lambda_1, 0\}).$$

where $\mathbf{x}_i$ is the ith element of a vector $\mathbf{x}$, $P_{[\check{c}_i, \hat{c}_i]}(\cdot)$ is the clip function over the interval $[\check{c}_i, \hat{c}_i]$.

The primal, dual feasibility and complementary slackness are

$$\lambda_1 = 0, \|\boldsymbol{\delta}\|_1 = \sum_{i=1}^d |\delta_i| = \sum_{i=1}^d |P_{[\check{c}_i, \hat{c}_i]}(a_i)| \leq \epsilon \tag{20}$$

$$\textbf{or } \lambda_1 > 0, \|\boldsymbol{\delta}\|_1 = \sum_{i=1}^d |\delta_i| = \sum_{i=1}^d |P_{[\check{c}_i, \hat{c}_i]}(\operatorname{sign}(a_i) \max\{|a_i| - \lambda_1, 0\})| = \epsilon. \tag{21}$$

If $\sum_{i=1}^d |P_{[\check{c}_i, \hat{c}_i]}(a_i)| \leq \epsilon$, $\delta_i^* = P_{[\check{c}_i, \hat{c}_i]}(a_i)$. Otherwise $\delta_i^* = P_{[\check{c}_i, \hat{c}_i]}(\operatorname{sign}(a_i) \max\{|a_i| - \lambda_1, 0\})$, where λ_1 is given by the root of the equation $\sum_{i=1}^d |P_{[\check{c}_i, \hat{c}_i]}(\operatorname{sign}(a_i) \max\{|a_i| - \lambda_1, 0\})| = \epsilon$. Bisection method can be used to solve the above equation for λ_1, starting with the initial interval $(0, \max_i |a_i| - \epsilon/d]$. Since $\sum_{i=1}^d |P_{[\check{c}_i, \hat{c}_i]}(\operatorname{sign}(a_i) \max\{|a_i| - 0, 0\})| = \sum_{i=1}^d |P_{[\check{c}_i, \hat{c}_i]}(a_i)| > \epsilon$ in this case, and $\sum_{i=1}^d |P_{[\check{c}_i, \hat{c}_i]}(\operatorname{sign}(a_i) \max\{|a_i| - \max_i |a_i| + \epsilon/d, 0\})| \leq \sum_{i=1}^d |P_{[\check{c}_i, \hat{c}_i]}(\operatorname{sign}(a_i)(\epsilon/d))| \leq \sum_{i=1}^d (\epsilon/d) = \epsilon$.

ℓ_2 **norm** When we find the Euclidean projection of $\mathbf{a}$ onto the set $\mathcal{X}$, we solve

$$\begin{array}{ll} \underset{\boldsymbol{\delta}}{\text{minimize}} & \|\boldsymbol{\delta} - \mathbf{a}\|_2^2 + I_{[\check{\mathbf{c}}, \hat{\mathbf{c}}]}(\boldsymbol{\delta}) \\ \text{subject to} & \|\boldsymbol{\delta}\|_2^2 \leq \epsilon^2, \end{array} \tag{22}$$

where $I_{[\check{\mathbf{c}}, \hat{\mathbf{c}}]}(\cdot)$ is the indicator function of the set $[\check{\mathbf{c}}, \hat{\mathbf{c}}]$. The Langragian of this problem is

$$L = \|\boldsymbol{\delta} - \mathbf{a}\|_2^2 + I_{[\check{\mathbf{c}}, \hat{\mathbf{c}}]}(\boldsymbol{\delta}) + \lambda_2(\|\boldsymbol{\delta}\|_2^2 - \epsilon^2) \tag{23}$$

$$= \sum_{i=1}^{d} ((\delta_i - a_i)^2 + \lambda_2 \delta_i^2 + I_{[\check{c}_i, \hat{c}_i]}(\delta_i)) - \lambda_2 \epsilon^2. \tag{24}$$

The minimizer $\boldsymbol{\delta}^*$ minimizes the Lagrangian, it is

$$\delta_i^* = P_{[\check{c}_i, \hat{c}_i]}(\frac{1}{\lambda_2 + 1} a_i).$$

The primal, dual feasibility and complementary slackness are

$$\lambda_2 = 0, \|\boldsymbol{\delta}\|_2^2 = \sum_{i=1}^{d} \delta_i^2 = \sum_{i=1}^{d} (P_{[\check{c}_i, \hat{c}_i]}(a_i))^2 \leq \epsilon^2 \tag{25}$$

$$\textbf{or } \lambda_2 > 0, \|\boldsymbol{\delta}\|_2^2 = \sum_{i=1}^{d} \delta_i^2 = (P_{[\check{c}_i, \hat{c}_i]}(\frac{1}{\lambda_2 + 1} a_i))^2 = \epsilon^2. \tag{26}$$

If $\sum_{i=1}^d (P_{[\check{c}_i, \hat{c}_i]}(a_i))^2 \leq \epsilon^2$, $\delta_i^* = P_{[\check{c}_i, \hat{c}_i]}(a_i)$. Otherwise $\delta_i^* = P_{[\check{c}_i, \hat{c}_i]}\left(\frac{1}{\lambda_2+1} a_i\right)$, where λ_2 is given by the root of the equation $\sum_{i=1}^d (P_{[\check{c}_i, \hat{c}_i]}(\frac{1}{\lambda_2+1} a_i))^2 = \epsilon^2$. Bisection method can be used to solve the above equation for λ_2, starting with the initial interval $(0, \sqrt{\sum_{i=1}^d (a_i)^2}/\epsilon - 1]$. Since $\sum_{i=1}^d (P_{[\check{c}_i, \hat{c}_i]}(\frac{1}{0+1} a_i))^2 = \sum_{i=1}^d (P_{[\check{c}_i, \hat{c}_i]}(a_i))^2 > \epsilon^2$ in this case, and $\sum_{i=1}^d (P_{[\check{c}_i, \hat{c}_i]}(\frac{1}{\lambda_2+1} a_i))^2 = \sum_{i=1}^d (P_{[\check{c}_i, \hat{c}_i]}(\epsilon a_i / \sqrt{\sum_{i=1}^d (a_i)^2}))^2 \leq \epsilon^2 \sum_{i=1}^d (a_i)^2 / (\sqrt{\sum_{i=1}^d (a_i)^2})^2 = \epsilon^2$.

ℓ_0 **norm** For ℓ_0 norm in $\mathcal{X}$, it is independent to the box constraint. So we can clip $\mathbf{a}$ to the box constraint first, which is $\delta_i' = P_{[\check{c}_i, \hat{c}_i]}(a_i)$, and then project it onto ℓ_0 norm.

We find the additional Euclidean distance of every element in $\mathbf{a}$ and zero after they are clipped to the box constraint, which is

$$\eta_i = \begin{cases} \sqrt{a_i^2 - (a_i - \check{c}_i)^2} & a_i < \check{c}_i \\ \sqrt{a_i^2 - (a_i - \hat{c}_i)^2} & a_i > \hat{c}_i \\ |a_i| & \text{otherwise.} \end{cases} \tag{27}$$

It can be equivalently written as

$$\eta_i = \begin{cases} \sqrt{2 a_i \check{c}_i - \check{c}_i^2} & a_i < \check{c}_i \\ \sqrt{2 a_i \hat{c}_i - \hat{c}_i^2} & a_i > \hat{c}_i \\ |a_i| & \text{otherwise.} \end{cases} \tag{28}$$

To derive the Euclidean projection onto ℓ_0 norm, we find the ϵ-th largest element in $\boldsymbol{\eta}$ and call it $[\boldsymbol{\eta}]_\epsilon$. We keep the elements whose corresponding η_i is above or equals to ϵ-th, and set rest to zeros. The closed-form solution is given by

$$\delta_i^* = \begin{cases} \delta_i' & \eta_i \geq [\boldsymbol{\eta}]_\epsilon \\ 0 & \text{otherwise.} \end{cases} \tag{29}$$

□

Difference with [25, Proposition 4.1]. We remark that [25] discussed a relevant problem of generating ℓ_p-norm based adversarial examples under box and linearized classification constraints. The key difference between our proof and that of [25, Proposition 4.1] is summarized below. First, we place ℓ_p norm as a hard constraint rather than minimizing it in the objective function. This difference will make our Lagrangian function more involved with a newly introduced non-negative Lagrangian multiplier. Second, the problem of our interest is projection onto the intersection of box and ℓ_p constraints. Such a projection step can then be combined with an attack loss (no need of linearization) for generating adversarial examples. Third, we cover the case of ℓ_0 norm.

B Proof of Lemma 1

Lemma 1. *Problem (11) is equivalent to*

$$\underset{\boldsymbol{\theta}}{\text{minimize}}\, \mathbb{E}_{(\mathbf{x},\mathbf{y})\in\mathcal{D}} \underset{\mathbf{w}\in\mathcal{P},\{\boldsymbol{\delta}_i\in\mathcal{X}_i\}}{\text{maximize}} \sum_{i=1}^{K} w_i f_{\text{tr}}(\boldsymbol{\theta}, \boldsymbol{\delta}_i; \mathbf{x}, y),$$

where $\mathbf{w} \in \mathbb{R}^K$ represent domain weights, and $\mathcal{P}$ has been defined in (1).

Proof of Lemma 1:

Similar to (1), problem (11) is equivalent to

$$\underset{\boldsymbol{\theta}}{\text{minimize}}\ \mathbb{E}_{(\mathbf{x},\mathbf{y})\in\mathcal{D}} \underset{\mathbf{w}\in\mathcal{P}}{\text{maximize}} \sum_{i=1}^{K} w_i F_i(\boldsymbol{\theta}). \tag{30}$$

Recall that $F_i(\boldsymbol{\theta}) := \text{maximize}_{\boldsymbol{\delta}_i\in\mathcal{X}_i}\ f_{\text{tr}}(\boldsymbol{\theta}, \boldsymbol{\delta}_i; \mathbf{x}, y)$, problem can then be written as

$$\underset{\boldsymbol{\theta}}{\text{minimize}}\ \mathbb{E}_{(\mathbf{x},\mathbf{y})\in\mathcal{D}} \underset{\mathbf{w}\in\mathcal{P}}{\text{maximize}} \sum_{i=1}^{K} [w_i \underset{\boldsymbol{\delta}_i\in\mathcal{X}_i}{\text{maximize}}\ f_{\text{tr}}(\boldsymbol{\theta}, \boldsymbol{\delta}_i; \mathbf{x}, y)]. \tag{31}$$

According to proof by contradiction, it is clear that problem (31) is equivalent to

$$\underset{\boldsymbol{\theta}}{\text{minimize}}\ \mathbb{E}_{(\mathbf{x},\mathbf{y})\in\mathcal{D}} \underset{\mathbf{w}\in\mathcal{P},\{\boldsymbol{\delta}_i\in\mathcal{X}_i\}}{\text{maximize}} \sum_{i=1}^{K} w_i f_{\text{tr}}(\boldsymbol{\theta}, \boldsymbol{\delta}_i; \mathbf{x}, y). \tag{32}$$

□

C Alternating Multi-step PGD (AMPGD) for Generalized AT

In this section, we present the full **a**lternating **m**ulti-step **p**rojected **g**radient **d**escent (AMPGD) algorithm to solve the problem (13), which is repeated as follows

$$\begin{array}{l} \underset{\boldsymbol{\theta}}{\text{minimize}}\ \mathbb{E}_{(\mathbf{x},\mathbf{y})\in\mathcal{D}}\ \underset{\mathbf{w}\in\mathcal{P},\{\boldsymbol{\delta}_i\in\mathcal{X}_i\}}{\text{maximize}}\ \psi(\boldsymbol{\theta},\mathbf{w},\{\boldsymbol{\delta}_i\}) \\ \psi(\boldsymbol{\theta},\mathbf{w},\{\boldsymbol{\delta}_i\}) := \sum_{i=1}^{K} w_i f_{\text{tr}}(\boldsymbol{\theta},\boldsymbol{\delta}_i;\mathbf{x},y) - \frac{\gamma}{2}\|\mathbf{w}-\mathbf{1}/K\|_2^2 \end{array}$$

Algorithm 3 AMPGD to solve problem (13)

```
1: Input: given $\boldsymbol{\theta}^{(0)}$, $\mathbf{w}^{(0)}$, $\boldsymbol{\delta}^{(0)}$ and $K > 0$.
2: for $t = 1, 2, \ldots, T$ do
3:     given $\mathbf{w}^{(t-1)}$ and $\boldsymbol{\delta}^{(t-1)}$, perform SGD to update $\boldsymbol{\theta}^{(t)}$
4:     given $\boldsymbol{\theta}^{(t)}$, perform $R$-step PGD to update $\mathbf{w}^{(t)}$ and $\boldsymbol{\delta}^{(t)}$
5: end for
```

Problem (13) is in a more general non-convex non-concave min-max setting, where the inner maximization involves both domain weights $\mathbf{w}$ and adversarial perturbations $\{\boldsymbol{\delta}_i\}$. It was shown in [46] that the multi-step PGD is required for inner maximization in order to approximate the near-optimal solution. This is also in the similar spirit of AT [40], which executed multi-step PGD attack during inner maximization. We summarize AMPGD in Algorithm 3. At step 4 of Algorithm 3, each PGD step to update $\mathbf{w}$ and $\boldsymbol{\delta}$ can be decomposed as

$$\begin{array}{l} \mathbf{w}_r^{(t)} = \text{proj}_{\mathcal{P}}\left(\mathbf{w}_{r-1}^{(t)} + \beta\nabla_{\mathbf{w}}\psi(\boldsymbol{\theta}^{(t)},\mathbf{w}_{r-1}^{(t)},\{\boldsymbol{\delta}_{i,r-1}^{(t)}\})\right), \forall r \in [R], \\ \boldsymbol{\delta}_{i,r}^{(t)} = \text{proj}_{\mathcal{X}_i}\left(\boldsymbol{\delta}_{i,r-1}^{(t)} + \beta\nabla_{\boldsymbol{\delta}}\psi(\boldsymbol{\theta}^{(t)},\mathbf{w}_{r-1}^{(t)},\{\boldsymbol{\delta}_{i,r-1}^{(t)}\})\right), \forall r, i \in [R], [K] \end{array}$$

where let $\mathbf{w}_1^{(t)} := \mathbf{w}^{(t-1)}$ and $\boldsymbol{\delta}_{i,1}^{(t)} := \boldsymbol{\delta}_i^{(t-1)}$. Here the superscript t represents the iteration index of AMPGD, and the subscript r denotes the iteration index of R-step PGD. Clearly, the above projection operations can be derived for closed-form expressions through (9) and Lemma 1. To the best of our knowledge, it is still an open question to build theoretical convergence guarantees for solving the general non-convex non-concave min-max problem like (13), except the work [46] which proposed $O(1/T)$ convergence rate if the objective function satisfies a strict Polyak-Łojasiewicz condition [29].

D Experiment Setup

D.1 Model Architectures and Training Details

For a comprehensive evaluation of proposed algorithms, we adopt a set of diverse DNN models (Model A to H), including multi-layer perceptrons (MLP), All-CNNs [61], LeNet [30], LeNetV2[3], VGG16 [58], ResNet50 [24], Wide-ResNet [40] and GoogLeNet [63]. For the last four models, we use the exact same architecture as original papers and evaluate them only on CIFAR-10 dataset. The details for model architectures are provided in Table A1. For compatibility with our framework, we implement and train these models based on the strategies adopted in pytorch-cifar[4] and achieve comparable performance on clean images; see Table A2. To foster reproducibility, all the trained models are publicly accessible in the anonymous link. Specifically, we trained MNIST classifiers for 50 epochs with Adam and a constant learning rate of 0.001. For CIFAR-10 classifers, the models are trained for 250 epochs with SGD (using 0.8 nesterov momentum, weight decay $5e^{-4}$). The learning rate is reduced at epoch 100 and 175 with a decay rate of 0.1. The initial learning rate is set as 0.01 for models {A, B, C, D, H} and 0.1 for {E, F, G}. Note that no data augmentation is employed in the training.

Table A1: Neural network architectures used on the MNIST and CIFAR-10 dataset. Conv: convolutional layer, FC: fully connected layer, Globalpool: global average pooling layer.

A (MLP)	**B** (All-CNNs [61])	**C** (LeNet [30])	**D** (LeNetV2)
FC(128) + Relu	Conv([32, 64], 3, 3) + Relu	Conv(6, 5, 5) + Relu	Conv(32, 3, 3) + Relu
FC(128) + Relu	Conv(128, 3, 3) + Dropout(0.5)	Maxpool(2, 2)	Maxpool(2, 2)
FC(64) + Relu	Conv([128, 128], 3, 3) + Relu	Conv(16, 5, 5) + Relu	Conv(64, 3, 3) + Relu
FC(10)	Conv(128, 3, 3) + Dropout(0.5)	Maxpool(2, 2)	Maxpool(2, 2)
Softmax	Conv(128, 3, 3) + Relu	FC(120) + Relu	FC(128) + Relu
	Conv(128, 1, 1) + Relu	FC(84) + Relu	Dropout(0.25)
	Conv(10, 1, 1) + Globalpool	FC(10)	FC(10)
	Softmax	Softmax	Softmax
E (VGG16 [58])	**F** (ResNet50 [24])	**G** (Wide-ResNet [40])	**H** (GoogLeNet [63])

Table A2: Clean test accuracy of DNN models on MNIST and CIFAR-10. We roughly derive the model robustness by attacking models separately using FGSM [23]. The adversarial examples are generated by FGSM ℓ_∞-attack ($\epsilon = 0.2$).

MNIST			CIFAR-10					
Model	Acc.	FGSM	Model	Acc.	FGSM	Model	Acc.	FGSM
A: MLP	98.20%	18.92%	A: MLP	55.36%	11.25%	E: VGG16	87.57%	10.83%
B: All-CNNs	99.49%	50.95%	B: All-CNNs	84.18%	9.89%	F: ResNet50	88.11%	10.73%
C: LeNet	99.25%	63.23%	C: LeNet	64.95%	14.45%	G: Wide-ResNet	91.67%	15.78%
D: LeNetV2	99.33%	56.36%	D: LeNetV2	74.89%	9.77%	H: GoogLeNet	90.92%	9.91%

D.2 Crafting Adversarial Examples

We adopt variant C&W loss in APGDA/PGD as suggested in [40, 13] with a confidence parameter $\kappa = 50$. Cross-entropy loss is also supported in our implementation. The adversarial examples are generated by 20-step PGD/APGDA unless otherwise stated (e.g., 50 steps for ensemble attacks). Note that proposed algorithms are robust and will not be affected largely by the choices of hyperparameters (α, β, γ). In consequence, we do not finely tune the parameters on the validation set. Specifically, The learning rates α, β and regularization factor γ for Table 1 are set as - $\ell_0 : \alpha = 1, \beta = \frac{1}{100}, \gamma = 7$, $\ell_1 : \alpha = \frac{1}{4}, \beta = \frac{1}{100}, \gamma = 5$, $\ell_2 : \alpha = \frac{1}{10}, \beta = \frac{1}{100}, \gamma = 3$; $\ell_\infty : \alpha = \frac{1}{4}, \beta = \frac{1}{50}, \gamma = 3$. For Table 3, the hyper-parameters are set as $\ell_0 : \alpha = 1, \beta = \frac{1}{150}, \gamma = 1$, $\ell_1 : \alpha = \frac{1}{4}, \beta = \frac{1}{100}, \gamma = 5$, $\ell_2 : \alpha = \frac{1}{8}, \beta = \frac{1}{100}, \gamma = 3$; $\ell_\infty : \alpha = \frac{1}{5}, \beta = \frac{1}{50}, \gamma = 6$.

[3] An enhanced version of original LeNet with more layers and units (see Table A1 Model D).

[4] https://github.com/kuangliu/pytorch-cifar

Due to varying model robustness on different datasets, the perturbation magnitudes ϵ are set separately [11]. For universal perturbation experiments, the ϵ are set as 0.2 (A, B), 0.3 (C) and 0.25 (D) on MNIST; 0.02 (B, H), 0.35 (E) and 0.05 (D) on CIFAR-10. For generalized AT, the models on MNIST are trained following the same rules in last section, except that training epochs are prolonged to 350 and adversarial examples are crafted for assisting the training with a ratio of 0.5. Our experiment setup is based on CleverHans package[5] and Carlini and Wagner's framework[6].

D.3 Details of Conducted Data Transformations

To demonstrate the effectiveness of APGDA in generating robust adversarial examples against multiple transformations, we adopt a series of common transformations, including a&b) flipping images horizontally (*flh*) and vertically (*flv*); c) adjusting image brightness (*bri*); d) performing gamma correction (*gam*), e) cropping and re-sizing images (*crop*); f) rotating images (*rot*).

Moreover, both deterministic and stochastic transformations are considered in our experiments. In particular, Table 7 and Table A5 are deterministic settings - *rot*: rotating images 30 degree clockwise; *crop*: cropping images in the center (0.8×0.8) and resizing them to 32×32; *bri*: adjusting the brightness of images with a scale of 0.1; *gam*: performing gamma correction with a value of 1.3. Differently, in Table A4, we introduce randomness for drawing samples from the distribution - *rot*: rotating images randomly from -10 to 10 degree; *crop*: cropping images in the center randomly (from 0.6 to 1.0); other transformations are done with a probability of 0.8. In experiments, we adopt `tf.image` API [7] for processing the images.

[5] `https://github.com/tensorflow/cleverhans`

[6] `https://github.com/carlini/nn_robust_attacks`

[7] `https://www.tensorflow.org/api_docs/python/tf/image`

E Additional Experiment Results - Robust adversarial attacks

E.1 Ensemble Attack over Multiple Models

Table 3 and A3 shows the performance of average (ensemble PGD [34]) and min-max (APGDA) strategies for attacking model ensembles. Our min-max approach results in 19.27% and 15.69% averaged improvement on ASR$_{all}$ over models {A, B, C, D} and {A, E, F, H} on CIFAR-10.

Table A3: Comparison of average and min-max (APGDA) ensemble attack over models {A, E, F, H} on CIFAR-10. Acc (%) represents the test accuracy of classifiers on adversarial examples. The learning rates α, β and regularization factor γ are set as - $\ell_0 : \alpha = 1, \beta = \frac{1}{150}, \gamma = 1$, $\ell_1 : \alpha = \frac{1}{4}, \beta = \frac{1}{100}, \gamma = 5$, $\ell_2 : \alpha = \frac{1}{8}, \beta = \frac{1}{100}, \gamma = 3$; $\ell_\infty : \alpha = \frac{1}{5}, \beta = \frac{1}{50}, \gamma = 6$. The attack iteration for APGDA is set as 50.

Box constraint	Opt.	Acc$_A$	Acc$_E$	Acc$_F$	Acc$_H$	ASR$_{all}$	Lift (↑)
ℓ_0 ($\epsilon = 70$)	*avg.*	27.38	6.33	7.18	6.99	66.56	-
	min max	19.38	8.72	9.48	8.94	**73.83**	**10.92%**
ℓ_1 ($\epsilon = 30$)	*avg.*	30.90	2.06	1.85	1.84	66.23	-
	min max	12.56	3.21	2.70	2.72	**83.13**	**25.52%**
ℓ_2 ($\epsilon = 1.5$)	*avg.*	20.87	1.75	1.21	1.54	76.41	-
	min max	10.26	3.15	2.24	2.37	**84.99**	**11.23%**
ℓ_∞ ($\epsilon = 0.03$)	*avg.*	25.75	2.59	1.66	2.27	70.54	-
	min max	13.47	3.79	3.15	3.48	**81.17**	**15.07%**

To perform a boarder evaluation, we repeat the above experiments (ℓ_∞ norm) under different ϵ in Figure A1. The ASR of min-max strategy is consistently better or on part with the average strategy. Moreover, APGDA achieves more significant improvement when moderate ϵ is chosen: MNIST ($\epsilon \in [0.15, 0.25]$) and CIFAR-10 ($\epsilon \in [0.03, 0.05]$).

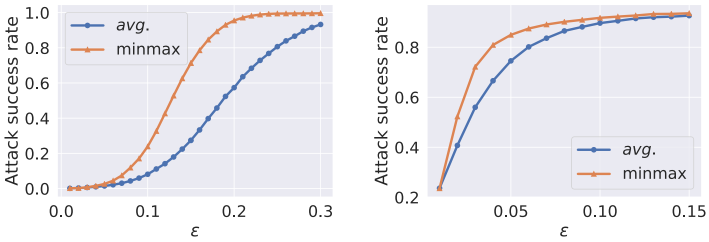

(a) MNIST {A, B, C}   (b) CIFAR-10 {A, B, C}

Figure A1: ASR of average and min-max ℓ_∞ ensemble attack versus maximum perturbation magnitude ϵ.

E.2 Robust Adversarial Attack over Data Transformations

Table A4 compare the performance of average (EOT [5]) and min-max (APGDA) strategies. Our approach results in 4.31% averaged lift over four models {A, B, C, D} on CIFAR-10 under given stochastic and deterministic transformation sets.

E.3 Analysis of Regularization on Probability Simplex

To further explore the utility of quadratic regularizer on the probability simplex in proposed min-max framework, we conducted sensitivity analysis on γ and show how the proposed regularization affects the eventual performance (Figure A2a) taking ensemble attack as an example. The experimental setting is the same as Table 1 except for altering the value of γ from 0 to 10. Figure A2a shows that too small or too large γ leads to relative weak performance due to the unstable convergence and penalizing too much for average case. When γ is around 4, APGDA will achieve the best performance so we adopted this value in the experiments (Table 1). Moreover, when $\gamma \to \infty$, the regularizer term dominates the optimization objective and it becomes the average case.

Table A4: Comparison of average and min-max optimization on robust attack over multiple data transformations on CIFAR-10. Note that all data transformations are conducted stochastically with a probability of 0.8, except for *crop* which randomly crops a central area from original image and re-size it into 32×32. The adversarial examples are generated by 20-step ℓ_∞-APGDA ($\epsilon = 0.03$) with $\alpha = \frac{1}{2}, \beta = \frac{1}{100}$ and $\gamma = 10$.

Model	Opt.	Acc$_{ori}$	Acc$_{flh}$	Acc$_{flv}$	Acc$_{bri}$	Acc$_{crop}$	ASR$_{avg}$	ASR$_{gp}$	Lift (↑)
A	*avg.*	11.55	21.60	13.64	12.30	22.37	83.71	55.97	-
	min max	13.06	18.90	13.43	13.90	20.27	84.09	**59.17**	**5.72%**
B	*avg.*	6.74	11.55	10.33	6.59	18.21	89.32	69.52	-
	min max	8.19	11.13	10.31	8.31	16.29	89.15	**71.18**	**2.39%**
C	*avg.*	8.23	17.47	13.93	8.54	18.83	86.60	58.85	-
	min max	9.68	13.45	13.41	9.95	18.23	87.06	**61.63**	**4.72%**
D	*avg.*	8.67	19.75	11.60	8.46	19.35	86.43	60.96	-
	min max	10.43	16.41	12.14	10.15	17.64	86.65	**63.64**	**4.40%**

Table A5: Comparison of average and min-max optimization on robust attack over multiple data transformations on CIFAR-10. Here a new rotation (*rot*) transformation is introduced, where images are rotated 30 degrees clockwise. Note that all data transformations are conducted with a probability of 1.0. The adversarial examples are generated by 20-step ℓ_∞-APGDA ($\epsilon = 0.03$) with $\alpha = \frac{1}{2}, \beta = \frac{1}{100}$ and $\gamma = 10$.

Model	Opt.	Acc$_{ori}$	Acc$_{flh}$	Acc$_{flv}$	Acc$_{bri}$	Acc$_{gam}$	Acc$_{crop}$	Acc$_{rot}$	ASR$_{avg}$	ASR$_{gp}$	Lift (↑)
A	*avg.*	11.06	22.37	14.81	12.32	10.92	20.40	15.89	84.60	49.24	-
	min max	13.51	18.84	14.03	15.20	13.00	18.03	14.79	84.66	**52.31**	**6.23%**
B	*avg.*	5.55	11.96	9.97	5.63	5.94	16.42	11.47	90.44	65.18	-
	min max	6.75	9.13	10.56	6.72	7.11	12.23	10.80	90.96	**70.38**	**7.98%**
C	*avg.*	7.65	22.30	15.82	8.17	8.07	15.44	15.09	86.78	49.67	-
	min max	9.05	15.10	14.57	9.57	9.31	14.11	14.23	87.72	**55.37**	**11.48%**
D	*avg.*	8.22	20.88	13.49	7.91	8.71	16.33	14.98	87.07	53.52	-
	min max	10.17	14.65	13.62	10.03	10.35	14.36	13.82	87.57	**57.36**	**7.17%**

F Additional Experiment Results - Adversarial training against multiple types of adversarial attacks

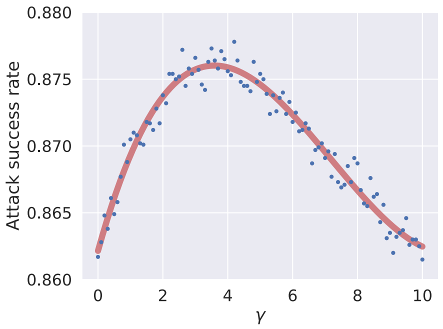

Figure A2: Sensitivity analysis of the regularizer $\frac{\gamma}{2}\|\mathbf{w} - \mathbf{1}/K\|_2^2$ on the probability simplex. The experimental setting is the same as Table 1 except for altering the value of γ.

Adversarial Training Details: Following the state-of-the-art approach MSD [41], we present experimental results of generalized AT to achieve simultaneous robustness to ℓ_∞, ℓ_2, and ℓ_1 perturbations on the MNIST and CIFAR-10 datasets. Specifically, we adopted the same architectures as [41] four layer convolutional networks on MNIST and the pre-activation version of the ResNet18 [24]. The perturbation radius ϵ for $(\ell_\infty, \ell_2, \ell_1)$ balls is set as $(0.3, 2.0, 10)$ and $(0.03, 0.5, 12)$ on MNIST and CIFAR-10 following [41]. For MNIST models, all models are trained 15 epochs with the Adam optimizer. We used a variation of the learning rate schedule from [60] - piecewise linear schedule from 0 to 10^{-3} over the first 6 epochs, and down to 0 over the last 9 epochs. For CIFAR-10 models, we trained all the models for 50 epochs and used the SGD optimizer with momentum 0.9 and weight decay 5×10^{-4}. The learning rate schedule rate is piecewise linear from 0 to 0.1 over the first 20 epochs, down to 0.005 over the next 20 epochs, and finally back down to 0 in the last 10 epochs.

Evaluation Setup: To make fair comparisons with MSD [41], we implemented AMPGD based on the public codebase[8] and followed the exact evaluation settings. Specifically, for ℓ_∞ attacks, we use FGSM [22], PGD attack [40] and Momentum Iterative Method [19]. For ℓ_2 attacks, we use PGD attack, the Gaussian noise attack [52], the boundary attack [9] (Brendel et al., 2017), DeepFool [45], the pointwise attack [55], DDN-based attack [54] and C&W attack [13]. For ℓ_1 attacks, we use the ℓ_1 PGD attack, the salt & pepper attack [52] and the pointwise attack [55]. Moreover, we also incorporate the state-of-the-art AutoAttack [18] for a more comprehensive evaluation under mixed ℓ_p perturbations.

Experimental Results: The complete adversarial accuracy results on ℓ_p attacks and the union of them are shown in Table A6. As we can see, our AMPGD approach leads to a consistent and significant improvement on MNIST. Compared to MSD, we found that our AMPGD emphasize more on defending the strongest adversary - ℓ_∞ PGD thus avoiding biased by one particular perturbation model. This observation is also consistent to the learning curves in Figure 3.

Table A6: Summary of adversarial robustness on MNIST.

	L_∞-AT	L_2-AT	L_1-AT	MAX [65]	AVG [65]	MSD [41]	AMPGD
Clean Accuracy	99.1%	99.2%	99.3%	98.6%	99.1%	98.3%	98.3%
ℓ_∞ Attacks ($\epsilon = 0.3$) [41]	90.3%	0.4%	0.0%	51.0%	65.2%	62.7%	76.1%
ℓ_2 Attacks ($\epsilon = 2.0$) [41]	13.6%	69.2%	38.5%	61.9%	60.1%	67.9%	70.2%
ℓ_1 Attacks ($\epsilon = 10$) [41]	4.2%	43.4%	70.0%	52.6%	39.2%	65.0%	67.2%
All Attacks [41]	3.7%	0.4%	0.0%	42.1%	34.9%	58.4%	**64.1%**
AA ($\ell_\infty, \epsilon = 0.3$) [18]	89.5%	0.0%	0.0%	55.0%	52.8%	56.6%	74.4%
AA ($\ell_2, \epsilon = 2.0$) [18]	3.5%	67.6%	37.3%	56.9%	55.8%	68.1%	63.8%
AA ($\ell_1, \epsilon = 10$) [18]	2.4%	60.1%	71.9%	46.5%	40.7%	70.0%	60.5%
AA (all attacks) [18]	1.7%	0.0%	0.0%	36.9%	30.5%	55.9%	**59.3%**
AA+ ($\ell_\infty, \epsilon = 0.3$) [18]	89.6%	0.0%	0.0%	54.4%	52.4%	55.7%	74.3%
AA+ ($\ell_2, \epsilon = 2.0$) [18]	2.1%	67.4%	36.8%	55.9%	53.8%	67.3%	61.9%
AA+ ($\ell_1, \epsilon = 10$) [18]	1.8%	60.4%	71.4%	42.3%	36.7%	68.6%	59.8%
AA+ (all attacks) [18]	1.2%	0.0%	0.0%	34.3%	28.8%	54.8%	**58.3%**

[8] https://github.com/locuslab/robust_union

G Interpreting “Image Robustness” with Domain Weights w

Tracking *domain weight* w of the probability simplex from our algorithms is an exclusive feature of solving problem 1. In Sec. 4, we show the strength of w in understanding the procedure of optimization and interpreting the adversarial robustness. Here we would like to show the usage of w in measuring “image robustness” on devising universal perturbation to multiple input samples. Table A7 and A8 show the image groups on MNIST with weight w in APGDA and two metrics (distortion of $\ell 2$-C&W, minimum ϵ for ℓ_∞-PGD) of measuring the difficulty of attacking single images. The binary search is utilized to searching for the minimum perturbation.

Although adversaries need to consider a trade-off between multiple images while devising universal perturbation, we find that weighting factor w in APGDA is highly correlated under different ℓ_p norms. Furthermore, w is also highly related to minimum distortion required for attacking a single image successfully. It means the inherent “image robustness” exists and effects the behavior of generating universal perturbation. Larger weight w usually indicates an image with higher robustness (e.g., fifth ’zero’ in the first row of Table A7), which usually corresponds to the MNIST letter with clear appearance (e.g., bold letter).

Table A7: Interpretability of domain weight w for universal perturbation to multiple inputs on MNIST (*Digit 0 to 4*). Domain weight w for different images under ℓ_p-norm ($p = 0, 1, 2, \infty$) and two metrics measuring the difficulty of attacking single image are recorded, where dist. (ℓ_2) denotes the the minimum distortion of successfully attacking images using C&W (ℓ_2) attack; $\epsilon_{\min}$ (ℓ_∞) denotes the minimum perturbation magnitude for ℓ_∞-PGD attack.

Image											
Weight	ℓ_0	0.	0.	0.	0.	1.000	0.248	0.655	0.097	0.	0.
	ℓ_1	0.	0.	0.	0.	1.000	0.07	0.922	0.	0.	0.
	ℓ_2	0.	0.	0.	0.	1.000	0.441	0.248	0.156	0.155	0.
	ℓ_∞	0.	0.	0.	0.	1.000	0.479	0.208	0.145	0.168	0.
Metric	dist.(C&W ℓ_2)	1.839	1.954	1.347	1.698	3.041	1.545	1.982	2.178	2.349	1.050
	$\epsilon_{\min}$ (ℓ_∞)	0.113	0.167	0.073	0.121	0.199	0.167	0.157	0.113	0.114	0.093
Image											
Weight	ℓ_0	0.	0.	0.613	0.180	0.206	0.	0.	0.223	0.440	0.337
	ℓ_1	0.	0.	0.298	0.376	0.327	0.	0.	0.397	0.433	0.169
	ℓ_2	0.	0.	0.387	0.367	0.246	0.	0.242	0.310	0.195	0.253
	ℓ_∞	0.087	0.142	0.277	0.247	0.246	0.	0.342	0.001	0.144	0.514
Metric	dist.(C&W ℓ_2)	1.090	1.182	1.327	1.458	0.943	0.113	1.113	1.357	1.474	1.197
	$\epsilon_{\min}$ (ℓ_∞)	0.075	0.068	0.091	0.105	0.096	0.015	0.090	0.076	0.095	0.106
Image											
Weight	ℓ_0	0.	1.000	0.	0.	0.	0.	0.	0.909	0.	0.091
	ℓ_1	0.	1.000	0.	0.	0.	0.	0.	0.843	0.	0.157
	ℓ_2	0.	0.892	0.	0.	0.108	0.	0.	0.788	0.	0.112
	ℓ_∞	0.	0.938	0.	0.	0.062	0.	0.	0.850	0.	0.150
Metric	dist.(C&W ℓ_2)	1.335	2.552	2.282	1.229	1.884	1.928	1.439	2.312	1.521	2.356
	$\epsilon_{\min}$ (ℓ_∞)	0.050	0.165	0.110	0.083	0.162	0.082	0.106	0.176	0.072	0.171
Image											
Weight	ℓ_0	0.481	0.	0.378	0.	0.	0.	0.352	0.	0.	0.648
	ℓ_1	0.690	0.	0.310	0.	0.	0.	0.093	0.205	0.	0.701
	ℓ_2	0.589	0.069	0.208	0.	0.134	0.064	0.260	0.077	0.	0.600
	ℓ_∞	0.864	0.	0.084	0.	0.052	0.079	0.251	0.156	0.	0.514
Metric	dist.(C&W ℓ_2)	2.267	1.656	2.053	1.359	0.861	1.733	1.967	1.741	1.031	2.413
	$\epsilon_{\min}$ (ℓ_∞)	0.171	0.088	0.143	0.117	0.086	0.100	0.097	0.096	0.038	0.132
Image											
Weight	ℓ_0	0.	0.	0.753	0.	0.247	0.	0.	0.	1.000	0.
	ℓ_1	0.018	0.	0.567	0.	0.416	0.347	0.	0.	0.589	0.063
	ℓ_2	0.	0.	0.595	0.	0.405	0.346	0.	0.	0.654	0.
	ℓ_∞	0.	0.	0.651	0.	0.349	0.239	0.	0.	0.761	0.
Metric	dist.(C&W ℓ_2)	1.558	1.229	1.939	0.297	1.303	0.940	1.836	1.384	1.079	2.027
	$\epsilon_{\min}$ (ℓ_∞)	0.084	0.088	0.122	0.060	0.094	0.115	0.103	0.047	0.125	0.100

Table A8: Interpretability of domain weight w for universal perturbation to multiple inputs on MNIST (*Digit 5 to 9*). Domain weight w for different images under ℓ_p-norm ($p = 0, 1, 2, \infty$) and two metrics measuring the difficulty of attacking single image are recorded, where dist. (ℓ_2) denotes the the minimum distortion of successfully attacking images using C&W (ℓ_2) attack; $\epsilon_{\min}$ (ℓ_∞) denotes the minimum perturbation magnitude for ℓ_∞-PGD attack.

Image											
Weight	ℓ_0	0.	0.062	0.254	0.	0.684	0.457	0.	0.	0.542	0.
	ℓ_1	0.131	0.250	0.	0.	0.619	0.033	0.157	0.005	0.647	0.158
	ℓ_2	0.012	0.164	0.121	0.	0.703	0.161	0.194	0.	0.508	0.136
	ℓ_∞	0.158	0.008	0.258	0.	0.576	0.229	0.179	0.	0.401	0.191
Metric	dist. (ℓ_2)	1.024	1.532	1.511	1.351	1.584	1.319	1.908	1.020	1.402	1.372
	$\epsilon_{\min}$ (ℓ_∞)	0.090	0.106	0.085	0.069	0.144	0.106	0.099	0.0748	0.131	0.071
Image											
Weight	ℓ_0	0.215	0.	0.	0.194	0.590	0.805	0.	0.	0.195	0.
	ℓ_1	0.013	0.	0.	0.441	0.546	0.775	0.	0.	0.225	0.
	ℓ_2	0.031	0.	0.	0.410	0.560	0.767	0.	0.	0.233	0.
	ℓ_∞	0.	0.	0.	0.459	0.541	0.854	0.	0.	0.146	0.
Metric	dist. (ℓ_2)	1.199	0.653	1.654	1.156	1.612	2.158	0.	1.063	1.545	0.147
	$\epsilon_{\min}$ (ℓ_∞)	0.090	0.017	0.053	0.112	0.158	0.159	0.020	0.069	0.145	0.134
Image											
Weight	ℓ_0	0.489	0.	0.	0.212	0.298	0.007	0.258	0.117	0.482	0.136
	ℓ_1	0.525	0.190	0.	0.215	0.070	0.470	0.050	0.100	0.343	0.038
	ℓ_2	0.488	0.165	0.	0.175	0.172	0.200	0.175	0.233	0.378	0.014
	ℓ_∞	0.178	0.263	0.	0.354	0.205	0.258	0.207	0.109	0.426	0.
Metric	dist. (ℓ_2)	1.508	1.731	1.291	1.874	1.536	1.719	2.038	1.417	2.169	0.848
	$\epsilon_{\min}$ (ℓ_∞)	0.110	0.125	0.089	0.126	0.095	0.087	0.097	0.084	0.135	0.077
Image											
Weight	ℓ_0	0.	0.	1.000	0.	0.	0.246	0.	0.	0.	0.754
	ℓ_1	0.	0.180	0.442	0.378	0.	0.171	0.	0.	0.	0.829
	ℓ_2	0.	0.298	0.593	0.109	0.	0.330	0.	0.	0.	0.670
	ℓ_∞	0.	0.377	0.595	0.028	0.	0.407	0.	0.	0.	0.593
Metric	dist. (ℓ_2)	1.626	1.497	1.501	1.824	0.728	1.928	1.014	1.500	1.991	1.400
	$\epsilon_{\min}$ (ℓ_∞)	0.070	0.153	0.156	0.156	0.055	0.171	0.035	0.090	0.170	0.161
Image											
Weight	ℓ_0	1.	0.	0.	0.	0.	0.	0.665	0.331	0.	0.004
	ℓ_1	0.918	0.	0.012	0.	0.070	0.	0.510	0.490	0.	0.
	ℓ_2	0.911	0.	0.089	0.	0.	0.	0.510	0.490	0.	0.
	ℓ_∞	0.935	0.	0.065	0.	0.	0.	0.665	0.331	0.	0.004
Metric	dist. (ℓ_2)	1.961	1.113	1.132	1.802	0.939	1.132	1.508	1.335	1.033	1.110
	$\epsilon_{\min}$ (ℓ_∞)	0.144	0.108	0.083	0.103	0.079	0.041	0.090	0.103	0.083	0.044